Supplemental Materials

Structural and transcriptomic alterations underlying the progression of aortic dissection in *Fbn1*$^{G234D/G234D}$ mice

Md Al Amin Sheikh, Kenichi Kimura, Eri Motoyama, Keiichi Asano, Violette Deleeuw, Patrick Sips, Chiho Tokunaga, Hiroko Matsunaga, Sachiko Kanki, Shigeki Koizumi, Kaori Sugiyama, Julie De Backer, Lynn Y Sakai, Haruko Takeyama, Yuji Hiramatsu, Haruka Ozaki, and Hiromi Yanagisawa

Supplementary table

Table S1: Human patient information used for RNA-seq analysis.

No.	Gender	Age	Diagnosis	Group	Operation
1	F	46	AR and AAE	Dilatation	Aortic root replacement (Bentall)
2	M	58	AR and AAE	Dilatation	Aortic root replacement (Bentall)
3	F	74	AR and Asc. aortic Dilatation	Dilatation	AVR and Ascending aorta replacement
4	F	72	AR and Asc. aortic Dilatation	Dilatation	AVR and Ascending aorta replacement
5	F	78	Subacute AD	Dissection	Ascending aorta replacement
6	F	54	Chronic AD	Dissection	Aortic root replacement (Bentall)
7	M	68	Chronic AD	Dissection	Hemiarch replacement

AR: aortic regurgitation; AAE: annuloaortic ectasia; AD: aortic dissection; Asc: Ascending; AVR: aortic valve replacement.

Supplemental Figures and Figure Legends

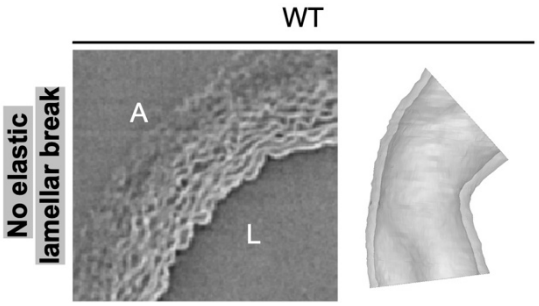

Figure S1. 3D segmentation of aortas from WT mice.
Representative synchrotron images of WT ascending aorta showing intact elastic lamellae (Left: Synchrotron image, right: 3D view of ascending aorta). n=10 mice. L: lumen, A: Adventitia.

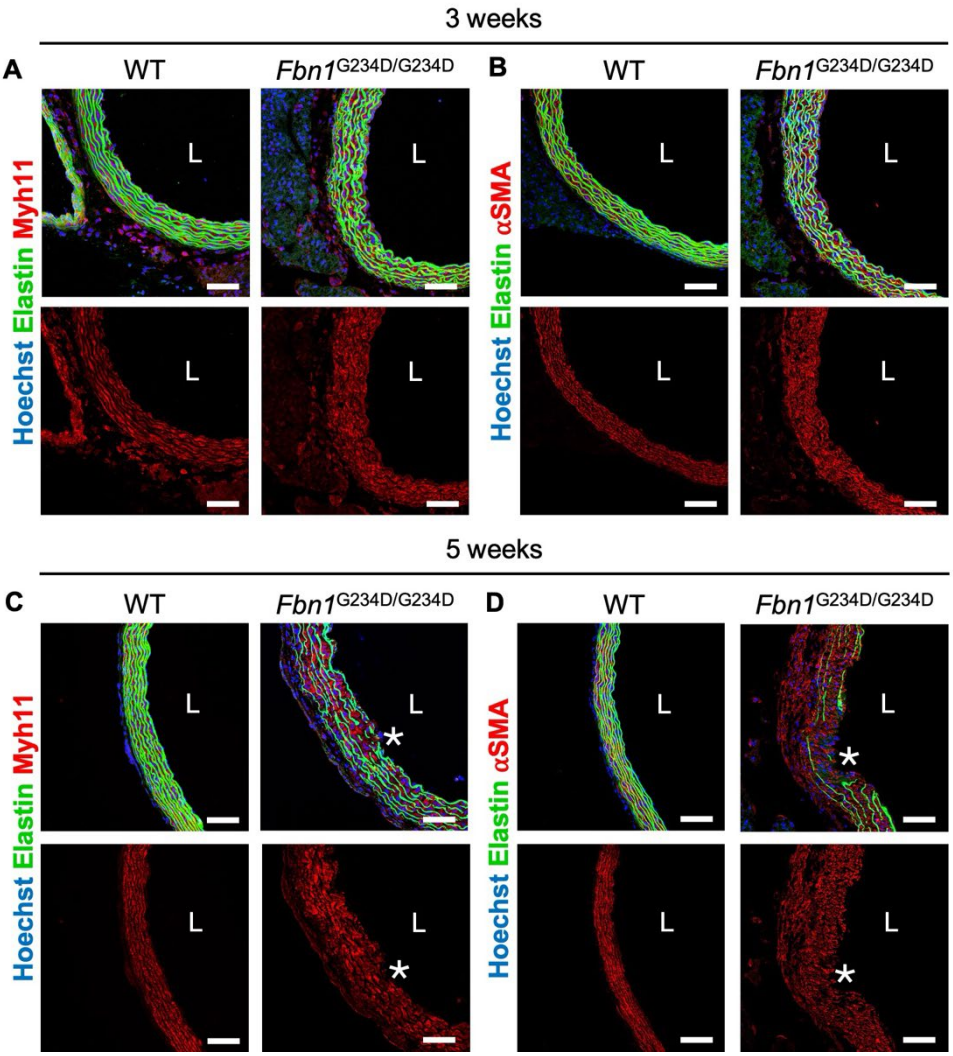

FigureS2. SMC contractile markers expression in WT and *Fbn1*$^{G234D/G234D}$ mice at 3 and 5 weeks.

Representative immunofluorescence images of cross-sections of ascending aortas from WT and *Fbn1*$^{G234D/G234D}$ mice at 3 weeks (A, B) and 5 weeks (C, D) of age. Sections were stained for Myh11 (A and C, red), αSMA (B and D, red), elastin autofluorescence (green), and Hoechst (blue). n=3 mice for each group. L: Lumen; *: Intimomedial tear, Scale bars: 50 μm.

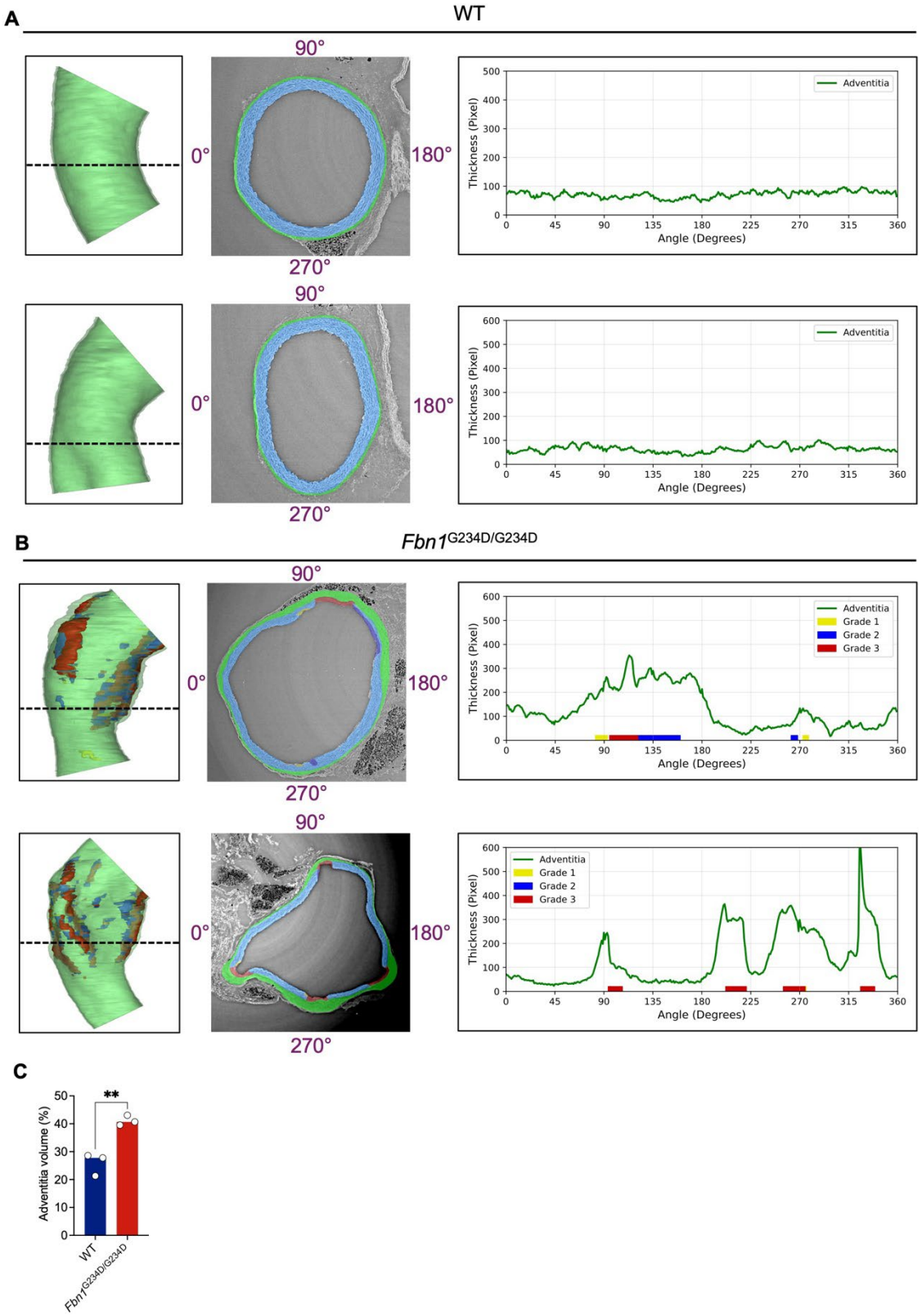

Figure S3. Extended analysis of adventitial wall thickness corresponding with intimomedial tear in WT and *Fbn1*$^{G234D/G234D}$ mice.

(A, B) Additional synchrotron-based 3D reconstructions, cross-sectional images, and circumferential thickness profiles of the ascending aortas from 5-week-old WT (A) and *Fbn1*$^{G234D/G234D}$ (B) mice. WT aortas exhibit consistent adventitial thickness with minimal regional variation, whereas *Fbn1*$^{G234D/G234D}$ aortas display adventitial thickening aligned with intimomedial tears. (C) Adventitia volume quantified as the percentage of total ascending aorta with adventitia at 5 weeks of age n=3 mice for each genotype. Data were shown as Mean ± SEM and analyzed by unpaired t-test. **p < 0.01

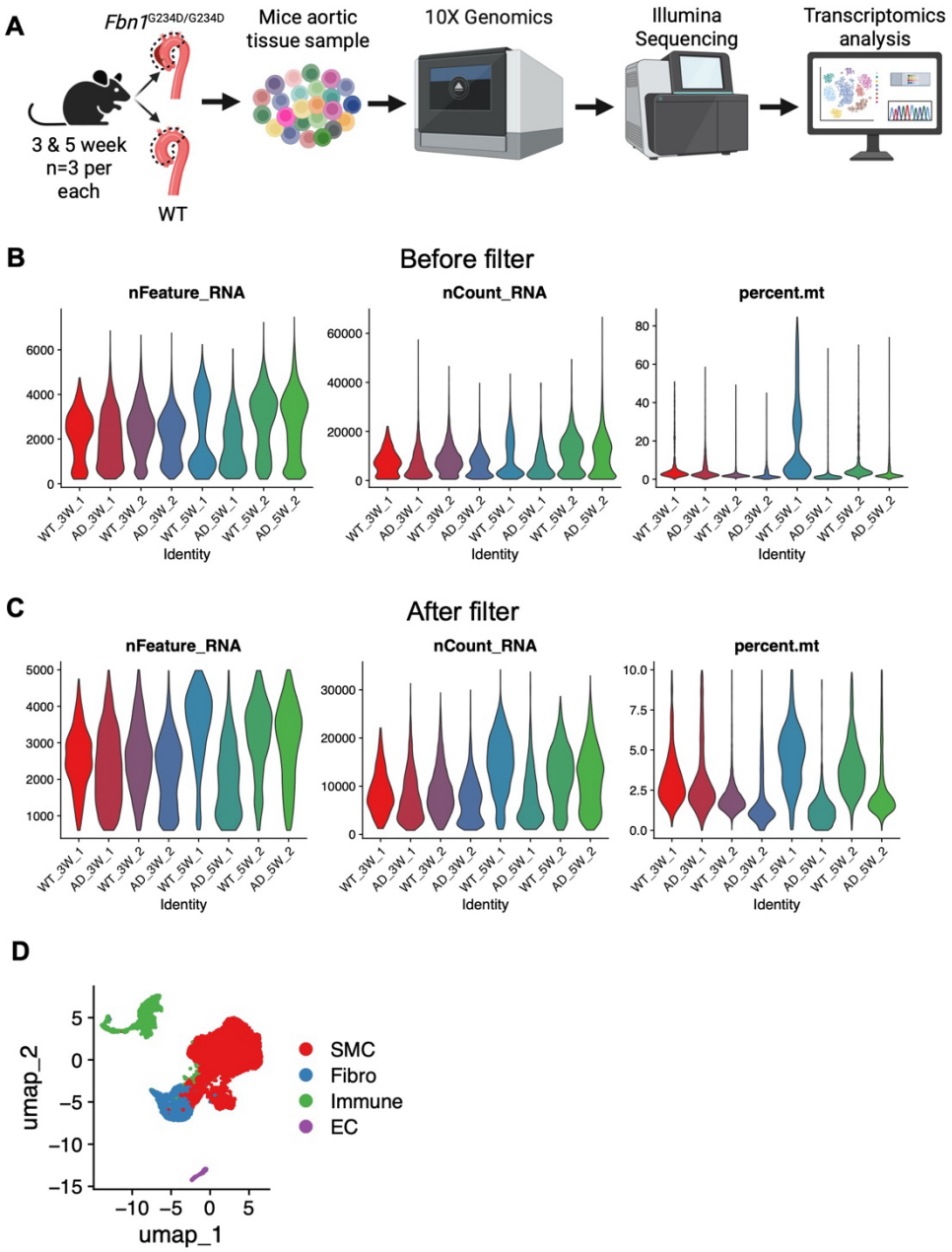

Figure S4. scRNA-seq of ascending aortas from WT and *Fbn1*$^{G234D/G234D}$ mice at 3 and 5 weeks of age.

(A) Schematic workflow of the scRNA-seq experiment. (B) Quality control (QC) metrics before filtering. Violin plots showing distributions of nFeatrue_RNA: Number of detected genes per cell, nCount_RNA: Total unique molecular identifiers (UMIs), percent.mt: Mitochondrial transcript content per cell (%), across all experimental groups with two biological replicates per group. (C) QC metrics after filtering with the filtering condition nFeature_RNA > 600, nFeature_RNA < 5000, and percent.mt < 10. (D) UMAP analysis of aortic cell populations and quality matrices. UMAP projection identified four major

aortic cell populations: smooth muscle cells (SMCs), fibroblasts (Fibro), immune cells, and endothelial cells (EC).